Growth of high spatial frequency periodic ripple structures on SiC crystal surfaces irradiated with successive femtosecond laser pulses

Go Obara,[1] Hisashi Shimizu,[1] Taira Enami,[1] Eric Mazur,[2] Mitsuhiro Terakawa,[1] and Minoru Obara[1,*]

[1]*School of Integrated Design Engineering, Keio University, 3-14-1, Hiyoshi, Kohoku-ku, Yokohama-shi, 223-8522, Japan*

[2]*Department of Physics, Harvard University, Cambridge, MA 02138, USA*

[*]*obara@obara.elec.keio.ac.jp*

Abstract: We present experimentally and theoretically the evolution of high spatial frequency periodic ripples (HSFL) fabricated on SiC crystal surfaces by irradiation with femtosecond laser pulses in a vacuum chamber. At early stages the seed defects are mainly induced by laser pulse irradiation, leading to the reduction in the ablation threshold fluence. By observing the evolution of these surface structures under illumination with successive laser pulses, the nanocraters are made by nanoablation at defects in the SiC surface. The Mie scattering by the nanoablated craters grows the periodic ripples. The number of HSFL is enhanced with increasing pulse number. At the edge of the laser spot the Mie scattering process is still dominant, causing the fabrication of HSFL. On the periphery of the spot SiC substrate remains a semiconductor state because the electron density in the SiC induced by laser irradiation is kept low. The HSFL observed is very deep in the SiC surface by irradiating with many laser pulses. These experimental results are well explained by 3D FDTD (three-dimensional finite-difference time-domain) simulation.

OCIS codes: (220.4241) Nanostructure fabrication; (350.3390) Laser materials processing; (290.4020) Mie theory; (250.5403) Plasmonics; (350.4238) Nanophotonics and photonic crystals.

References and links

1. D. Schurig, J. J. Mock, B. J. Justice, S. A. Cummer, J. B. Pendry, A. F. Starr, and D. R. Smith, "Metamaterial electromagnetic cloak at microwave frequencies," Science **314**(5801), 977–980 (2006).
2. J. D. Joannopoulos, P. R. Villeneuve, and S. Fan, "Photonic crystals: Putting a new twist on light," Nature **386**(6621), 143–149 (1997).
3. J. Hiller, J. D. Mendelsohn, and M. F. Rubner, "Reversibly erasable nanoporous anti-reflection coatings from polyelectrolyte multilayers," Nat. Mater. **1**(1), 59–63 (2002).
4. M. Birnbaum, "Semiconductor surface damage produced by ruby lasers," J. Appl. Phys. **36**(11), 3688–3689 (1965).
5. J. E. Sipe, J. F. Young, J. Preston, and H. van Driel, "Laser-induced periodic surface structure. I. Theory," Phys. Rev. B **27**(2), 1141–1154 (1983).
6. J. F. Young, J. F. Preston, H. M. van Driel, and J. E. Sipe, "Laser-induced periodic surface structure. II. Experiments on Ge, Si, Al, and brass," Phys. Rev. B **27**(2), 1155–1172 (1983).
7. J. F. Young, J. E. Sipe, and H. van Driel, "Laser-induced periodic surface structure. III. Fluence regimes, the role of feedback, and details of the induced topography in germanium," Phys. Rev. B **30**(4), 2001–2015 (1984).
8. M. Ezaki, H. Kumagai, K. Toyoda, and M. Obara, "Surface modification of III-V compound semiconductors using surface electromagnetic wave etching induced by ultraviolet lasers," IEEE J. Sel. Top. Quantum Electron. **1**(3), 841–847 (1995).
9. D. Dufft, A. Rosenfeld, S. K. Das, R. Grunwald, and J. Bonse, "Femtosecond laser-induced periodic surface structures revisited: a comparative study on ZnO," J. Appl. Phys. **105**(3), 034908 (2009).
10. N. Tagawa, M. Takada, A. Mori, H. Sawada, and K. Kawahara, "Development of contact sliders with nanotextures by femtosecond laser processing," Tribol. Lett. **24**(2), 143–149 (2006).

#196394 - $15.00 USD Received 26 Aug 2013; revised 11 Oct 2013; accepted 15 Oct 2013; published 25 Oct 2013

11. B. Wu, M. Zhou, J. Li, X. Ye, G. Li, and L. Cai, "Superhydrophobic surfaces fabricated by microstructuring of stainless steel using a femtosecond laser," Appl. Surf. Sci. **256**(1), 61–66 (2009).
12. X. Wang, C. A. Ohlin, Q. Lu, and J. Hu, "Cell directional migration and oriented division on three-dimensional laser-induced periodic surface structures on polystyrene," Biomaterials **29**(13), 2049–2059 (2008).
13. Y. Yang, J. Yang, C. Liang, H. Wang, X. Zhu, and N. Zhang, "Surface microstructuring of Ti plates by femtosecond lasers in liquid ambiences: a new approach to improving biocompatibility," Opt. Express **17**(23), 21124–21133 (2009).
14. B. Dusser, Z. Sagan, H. Soder, N. Faure, J. P. Colombier, M. Jourlin, and E. Audouard, "Controlled nanostructrures formation by ultra fast laser pulses for color marking," Opt. Express **18**(3), 2913–2924 (2010).
15. A. Y. Vorobyev, V. S. Makin, and C. Guo, "Brighter light sources from black metal: Significant increase in emission efficiency of incandescent light sources," Phys. Rev. Lett. **102**(23), 234301 (2009).
16. E. D. Diebold, N. H. Mack, S. K. Doorn, and E. Mazur, "Femtosecond laser-nanostructured substrates for surface-enhanced Raman scattering," Langmuir **25**(3), 1790–1794 (2009).
17. A. Hamdorf, M. Olson, C.-H. Lin, L. Jiang, J. Zhou, H. Xiao, and H.-L. Tsai, "Femtosecond and nanosecond laser fabricated substrate for surface-enhanced Raman scattering," Opt. Lett. **36**(17), 3353–3355 (2011).
18. J. Bonse, A. Rosenfeld, and J. Krüger, "On the role of surface plasmon polaritons in the formation of laser induced periodic surface structures upon irradiation of silicon by femtosecond laser pulse," J. Appl. Phys. **106**(10), 104910 (2009).
19. M. Huang, F. Zhao, Y. Cheng, N. Xu, and Z. Xu, "Origin of laser-induced near-subwavelength ripples: interference between surface plasmons and incident laser," ACS Nano **3**(12), 4062–4070 (2009).
20. G. Miyaji and K. Miyazaki, "Origin of periodicity in nanostructuring on thin film surfaces ablated with femtosecond laser pulses," Opt. Express **16**(20), 16265–16271 (2008).
21. G. Obara, N. Maeda, T. Miyanishi, M. Terakawa, N. N. Nedyalkov, and M. Obara, "Plasmonic and Mie scattering control of far-field interference for regular ripple formation on various material substrates," Opt. Express **19**(20), 19093–19103 (2011).
22. M. Huang, F. Zhao, Y. Cheng, N. Xu, and Z. Xu, "Mechanisms of ultrafast laser-induced deep-subwavelength gratings on graphite and diamond," Phys. Rev. B **79**(12), 125436 (2009).
23. S. Sakabe, M. Hashida, S. Tokita, S. Namba, and K. Okamuro, "Mechanism for self-formation of periodic grating structures on a metal surface by a femtosecond laser pulse," Phys. Rev. B **79**(3), 033409 (2009).
24. S. K. Das, D. Dufft, A. Rosenfeld, J. Bonse, M. Bock, and R. Grunwald, "Femtosecond-laser-induced quasi periodic nanostructures on TiO_2 surfaces," J. Appl. Phys. **105**(8), 084912 (2009).
25. R. Le Harzic, D. Dörr, D. Sauer, M. Neumeier, M. Epple, H. Zimmermann, and F. Stracke, "Large-area, uniform, high-spatial-frequency ripples generated on silicon using a nanojoule-femtosecond laser at high repetition rate," Opt. Lett. **36**(2), 229–231 (2011).
26. Q. Sun, F. Liang, R. Vallée, and S. L. Chin, "Nanograting formation on the surface of silica glass by scanning focused femtosecond laser pulses," Opt. Lett. **33**(22), 2713–2715 (2008).
27. F. Liang, R. Vallée, and S. L. Chin, "Mechanism of Nanograting formation on the surface of fused silica," Opt. Express **20**(4), 4389–4396 (2012).
28. V. R. Bhardwaj, E. Simova, P. P. Rajeev, C. Hnatovsky, R. S. Taylor, D. M. Rayner, and P. B. Corkum, "Optically produced arrays of planar nanostructures inside fused silica," Phys. Rev. Lett. **96**(5), 057404 (2006).
29. Y. Shimotsuma, P. G. Kazansky, J. Qiu, and K. Hirao, "Self-organized nanogratings in glass irradiated by ultrashort light pulses," Phys. Rev. Lett. **91**(24), 247405 (2003).
30. E. M. Hsu, T. H. Crawford, C. Maunders, G. A. Botton, and H. K. Haugen, "Cross-sectional study of periodic surface structures on gallium phosphide induced by ultrashort laser pulse irradiation," Appl. Phys. Lett. **92**(22), 221112 (2008).
31. S. H. Kim, I. B. Sohn, and S. Jeong, "Fabrication of uniform nanogrooves on 6H-SiC by femtosecond laser ablation," Appl. Phys., A Mater. Sci. Process. **102**(1), 55–59 (2011).
32. M. Yamaguchi, S. Ueno, R. Kumai, K. Kinoshita, T. Murai, T. Tomita, S. Matsuo, and S. Hashimoto, "Raman spectroscopic study of femtosecond laser-induced phase transformation associated with ripple formation on single-crystal SiC," Appl. Phys., A Mater. Sci. Process. **99**(1), 23–27 (2010).
33. A. V. Emelyanov, A. G. Kazanskii, P. K. Kashkarov, O. I. Konkov, E. I. Terukov, P. A. Forsh, M. V. Khenkin, A. V. Kukin, M. Beresna, and P. Kazansky, "Effect of the femtosecond laser treatment of hydrogenated amorphous silicon films on their structural, optical, and photoelectric properties," Semiconductors **46**(6), 749–754 (2012).
34. J. Bonse, S. Baudach, J. Krüger, W. Kautek, and M. Lenzner, "Femtosecond laser ablation of silicon-modification thresholds and morphology," Appl. Phys., A Mater. Sci. Process. **74**(1), 19–25 (2002).
35. T. Tomita, K. Kinoshita, S. Matsuo, and S. Hashimoto, "Effect of surface roughening on femtosecond laser-induced ripple structures," Appl. Phys. Lett. **90**(15), 153115 (2007).
36. E. D. Palik, *Handbook of Optical Constants of Solids* (Academic, 1998).
37. N. T. Son, W. M. Chen, O. Kordina, A. O. Konstantinov, B. Monemar, E. Janzén, D. M. Hofman, D. Volm, M. Drechsler, and B. K. Meyer, "Electron effective masses in 4H SiC," Appl. Phys. Lett. **66**(9), 1074–1076 (1995).
38. S.-H. Cho, H. Kumagai, K. Midorikawa, and M. Obara, "Fabrication of double cladding structure in optical multimode fibers using plasma channeling excited by a high-intensity femtosecond laser," Opt. Commun. **168**(1-4), 287–295 (1999).

#196394 - $15.00 USD Received 26 Aug 2013; revised 11 Oct 2013; accepted 15 Oct 2013; published 25 Oct 2013

39. N. Bloembergen, "Role of cracks, pores, and absorbing inclusions on laser induced damage threshold at surfaces of transparent dielectrics," Appl. Opt. **12**(4), 661–664 (1973).
40. L. G. DeShazer, B. E. Newnam, and K. M. Leung, "Role of coating defects in laser-induced damage to dielectric thin films," Appl. Phys. Lett. **23**(11), 607–609 (1973).
41. S. Martin, A. Hertwig, M. Lenzner, J. Krüger, and W. Kautek, "Spot-size dependence of the ablation threshold in dielectrics for femtosecond laser pulses," Appl. Phys., A Mater. Sci. Process. **77**, 883–884 (2003).

1. Introduction

Materials embedded with periodic structures of less than the incident optical wavelength become photonic functional materials inclusive of metamaterials [1], photonic crystals [2], antireflection films [3], etc. Short wavelength lasers and electron beams have widely been used to manufacture micro/nano structures beyond the diffraction limit. The ArF excimer laser exposure at the ultraviolet wavelength of 193 nm has been used for the two-dimensional processing of ULSI (ultra-large scale integration) devices. The photolithography is a very useful and industrial technique, and arbitrary patterns of the size of 1/10 of the wavelength are actually accomplished using 193-nm ArF laser.

On the other hand, the dry etching process at the submicrometer scale for a large area surface is desired. Laser ablation processing to fabricate these structures in the period of the submicrometer scale is extensively studied: There are periodic ripples produced via a self-organization process when many pulses of pulsed laser are irradiated. In 1965 it is reported by Birnbaum that the optical damage on the semiconductor surfaces is induced by a pulsed ruby laser [4]. Sipe and others reported experimentally and theoretically that the periodic structures are fabricated on Ge, Si, Al, and brass substrates by 20-ns Q-switched Nd:YAG laser pulses [5–7]. This structure formation is explained by surface scattering model caused by the surface roughness. Recently this ripple is called low spatial frequency LIPSS (Laser-Induced Periodic Surface Structure), which is formed perpendicularly to the polarization of the incident laser, and the periodicity is approximately the incident laser wavelength. Ezaki and others manufactured accurate ripple structures and 2D arrays in an etching gas atmosphere by illumination with two laser beam interference [8]. More recently, high spatial frequency LIPSS with a quarter periodicity of the illuminated wavelength is fabricated on ZnO substrate by femtosecond laser illumination [9].

The periodic ripple structured surfaces are applied to friction reduction [10], surface water-repellent/hydrophilic property [11], control of the cell growth direction [12], biocompatible improvement [13], structural color [14], control of the surface reflection [15], SERS (Surface-Enhanced Raman Spectroscopy), etc [16,17]. Conventionally made LIPSS had a distortion and undulation in a periodic ripple and is not an accurate periodic structure [9]. Therefore, the application to the field of surface optical device was technically difficult. The elucidation of the periodic structure formation physics is expected and the high spatial frequency LIPSS is highly desired, because the accurate micro/nanogroove structure will be applied to the surface photonic devices.

The underlying physics for LSFL (Low Spatial Frequency LIPSS) formation has been discussed in the literature. Bonse et al. [18] and Huang et al. [19] reported the surface plasmon polaritons generated by surface roughness form LSFL. Miyaji et al. [20] also reported the LSFL formation on DLC thin film is caused by surface plasmon polaritons. The irradiated laser may be scattered by inherent surface roughness. For example, the silicon surface will turn to be metallic during femtosecond laser irradiation, because the free electron density in silicon excited by intense femtosecond laser irradiation is increased up to the critical density determined by the laser wavelength. Hence spatially modulated intensity pattern is generated by plasmonically scattered far field interfered with the incident laser. We have previously reported the control of the LIPSS pattern formation by controlling the optical intensity distribution of plasmonic far-field with an arbitrary nano plasmon polaritons generator template [21].

#196394 - $15.00 USD Received 26 Aug 2013; revised 11 Oct 2013; accepted 15 Oct 2013; published 25 Oct 2013

However, the background physics for HSFL (High Spatial Frequency LIPSS) is not understood accurately. Dufft et al. fabricated LSFL and HSFL on the ZnO substrate (Eg = 3.37 eV) by Gaussian-profile femtosecond laser irradiation at average fluence of 0.62 J/cm^2 and 10 pulses [9]. LSFL is formed in the center of the irradiated spot, while HSFL is formed on the periphery. At low average fluence of 0.48 J/cm^2 and 50 pulses, only HSFL is formed in the entire area. HSFL is formed experimentally at relatively lower fluence than that for the LSFL formation.

Hypotheses for HSFL formation are proposed, which are due to surface plasmon [22, 23], second harmonic wave [24, 25], etc. HSFL is formed on various material surfaces of Si [25], ZnO [9], TiO_2 [24] and SiO_2 [26] with the fundamental wave and the second harmonic wave of femtosecond laser. Liang et al. reported that the width and spacing of grooves decrease with the increase of the number overlapped shots in both stationary and scanning cases [27]. Nanostructure inscription inside fused silica by Corkum group [28] and Hirao group [29] has been reported. We consider that this research is in a different research stream, because plasma waves are interacted in highly confined laser-induced plasma. On GaP substrate surfaces, the depth of the formed HSFL is more than one micrometer [30]. On 6H-SiC surfaces, HSFL is fabricated with a high aspect ratio [31]. The area where LSFL is formed contains both crystalline and amorphous layer on the SiC crystal surface, while the area of HSFL consists of only an amorphous layer [32].

The phase transition of electronic materials has previously been studied using femtosecond laser irradiation: The recrystallization is governed by the cooling rate of the molten phase [33]. The formed HSFL area exists on the periphery of the irradiated spot. The cooling velocity seems high, because the HSFL area is narrow and irradiated with lower fluence laser. This is likely to be the reason why the HSFL area changes to the amorphous layer. As for a single crystal Si wafer irradiated with Gaussian-profile femtosecond laser, the center of the irradiated spot is ablated, the outer of the ablated area is recrystallized, and the edge of the spot is converted to be amorphous [34]. For HSFL fabrication, the electron density produced by femtosecond laser irradiation does not exceed the critical density which is determined by the irradiation wavelength.

The threshold fluence for the HSFL formation depends on the density and size of the surface roughness [35]. Tomita et al. studied the effect of surface roughness on the threshold fluence for LIPSS formation for various surface roughened SiC wafers (Eg = 3.2 eV) [35]. The experimental result suggests that the threshold fluence for LSFL is not affected by surface roughness. Conversely the threshold fluence for HSFL formation is reduced by the surface roughness, compared to the mirror-like surface wafer. As described previously, surface roughness may act as a scatterer of the irradiated light. However, it is still not known how the initial surface nano-structure affects the growth of the HSFL.

We present experimentally and theoretically the evolution of HSFL by successive laser pulse irradiation. We irradiated nitrogen-doped single crystal 4H-SiC (0001) wafers with femtosecond laser. 4H-SiC is a wide bandgap material (Eg = 3.2 eV) and a next generation functional material for power switching device for electric vehicle and electric train due to its higher voltage performance than that of silicon crystal. We observed the evolution of these structures growth under the illumination with successive laser pulses. We also simulated optical intensity distributions on the SiC surfaces to explain the HSFL formation by 3D FDTD (three-dimensional finite-difference time-domain) method.

2. Simulation procedure

We simulate the distribution of optical field enhancement by 3D FDTD method, whose software package is commercially available (Poynting, Fujitsu, Co., Japan). As shown in Fig. 1, we place a ripple structure of rod-like crater on the SiC surface in the simulation system to analyze the optical field distribution. The laser source is a linearly polarized plane wave, being 800 nm above the SiC substrate. The center wavelength of the laser is 800 nm of

#196394 - $15.00 USD Received 26 Aug 2013; revised 11 Oct 2013; accepted 15 Oct 2013; published 25 Oct 2013

Ti:Al_2O_3 femtosecond laser, which is incoming vertically to the SiC substrate. The incident electric field strength is assumed as 1V/m. The 800-nm laser illuminates uniformly a large area of 5000 x 5000 nm^2, and the minimum cell size of FDTD simulation is 5 x 5 x 5 nm^3. First order Mur absorption boundary condition is applied on the surfaces normal to *z* axis, and periodic boundary condition is applied on surfaces normal to *x* and *y* axes. The simulated field intensity distributions at 27 fs of pulse duration are shown in this paper. The time of 27 fs is at which electric field on the surface becomes a steady state. The optical intensity is calculated as an average value of one cycle optical wave (2.7 fs for 800 nm). Optical constants of materials used in the simulation are taken from [18,36,37]. Optical constant for SiC semiconductor is n = 2.605 + 0i and that for metal-like SiC is n = 1.272 + 1.028i at Ne = 1.14 x $10^{21}cm^{-3}$.

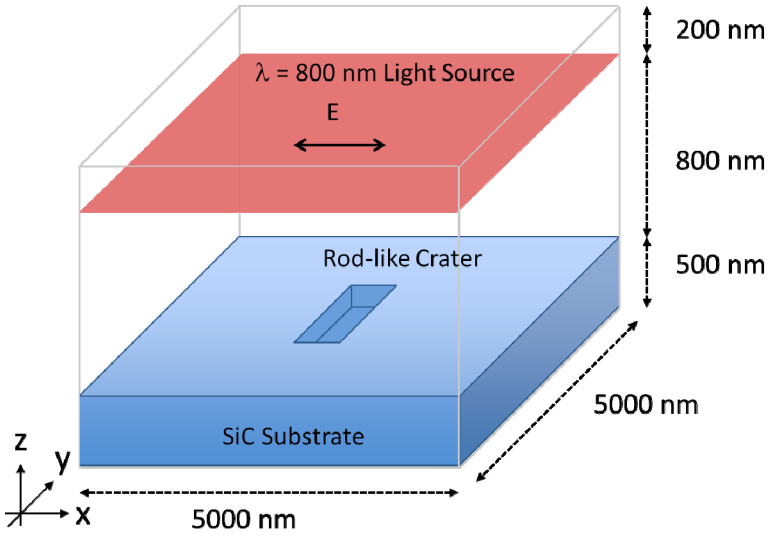

Fig. 1. Schematic of 3D FDTD simulation system. Small rod-like crater is centered on 4H-SiC substrate.

3. Experimental

We irradiated N-doped 4H SiC (0001) wafers with Ti:Al_2O_3 femtosecond laser pulses (λ = 800 nm (1.55 eV), τ = 150 fs, 100 Hz) at normal incidence in a vacuum chamber at 26.6 Pa (0.20 Torr). The pulse number was controlled by a mechanical shutter. The beam diameter of ω_o = 284 μm x 324 μm was measured at $1/e^2$ of the peak intensity with CCD camera. We used an average fluence.

4. Results and discussion

Figure 2 shows pulse number dependence of the optical damage threshold for SiC surface by 150 fs femtosecond laser irradiation. The optically-damaged area is measured by optical microscope. The damage threshold fluence is determined at which no damage is observed. As shown in Fig. 2, the damage threshold is decreased as the irradiation pulse number is increased. This result is due to the incubation effect. The experimental damage threshold is proportional to $N^{-0.33}$ (N: pulse number). It is likely to create the defects such as color center by successive laser pulse irradiation [38]. The damage threshold is reduced mainly by net optical absorption of the created surface defects [38].

#196394 - $15.00 USD Received 26 Aug 2013; revised 11 Oct 2013; accepted 15 Oct 2013; published 25 Oct 2013

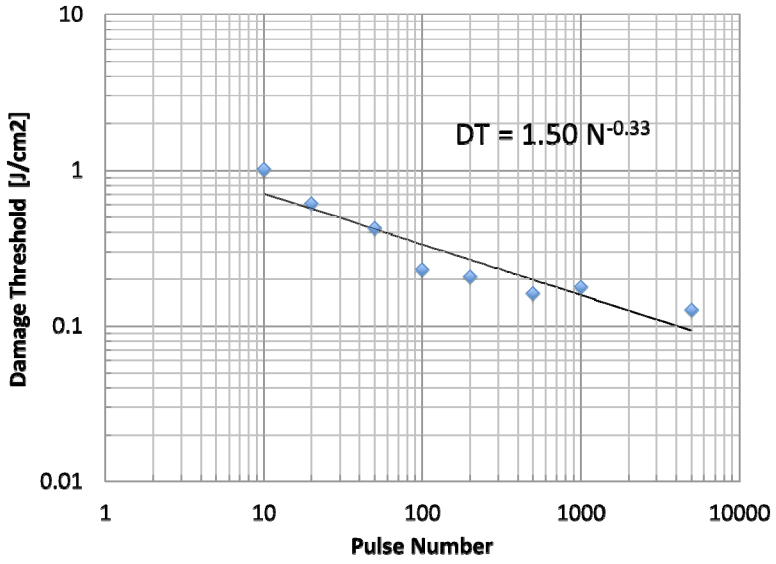

Fig. 2. Pulse number dependence of laser damage threshold for 4H-SiC by femtosecond laser pulse. DT: damage threshold, N: pulse number.

Surface damage threshold depends on the defect formation [39], defect density [40] and beam spot size [41]. The result shown in Fig. 2 is also due to the optical absorption and scattering at created surface defects. As a result, the damage threshold decreases with increasing laser pulse number.

Figure 3 shows SEM images of the SiC surface after the laser irradiation. As it is shown in Fig. 3(b), the ablated area seems similar to the irradiate laser beam diameter of 284 μm x 324 μm. Especially, linear cracks shown in (a) and (c) are observed inside the beam spot.

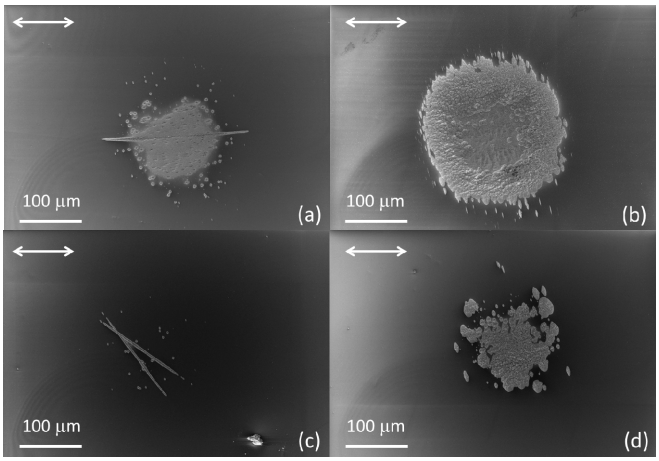

Fig. 3. SEM images of the 4H-SiC surfaces after the femtosecond laser irradiation. (a) F = 0.4 J/cm^2, 100 pulses, (b) F = 0.4 J/cm^2, 500 pulses, (c) F = 0.3 J/cm^2, 100, and (d) F = 0.3 J/cm^2, 500 pulses. White arrow shows the electric field vector of the incident laser.

#196394 - $15.00 USD Received 26 Aug 2013; revised 11 Oct 2013; accepted 15 Oct 2013; published 25 Oct 2013

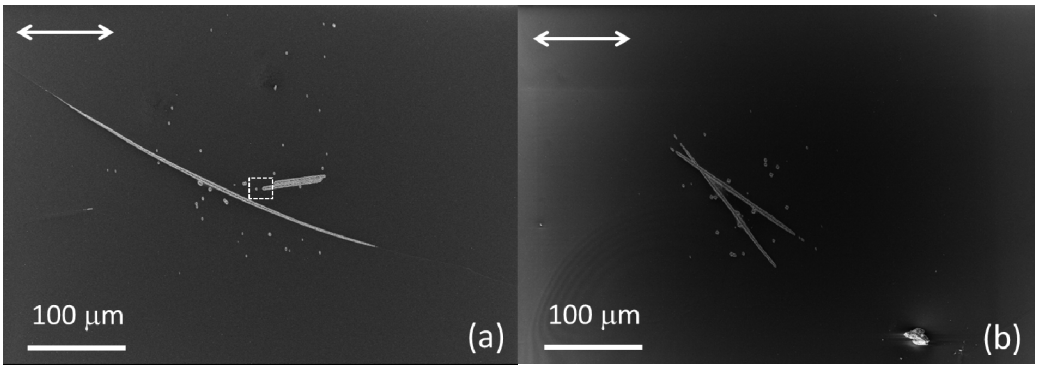

Fig. 4. SEM images of the 4H-SiC surfaces after the femtosecond laser irradiation at 0.3 J/cm^2. (a) 50 pulses, (b) 100 pulses. White arrow represents the electric field vector of the incident laser.

Figure 4 shows SEM images of the SiC surfaces after laser irradiation with 0.3 J/cm^2, 50 pulses and 100 pulses. Both experimental results have the same crack formed in the irradiated area and the cracks are randomly formed on the substrate surfaces. Figure 5 shows the magnified SEM images of the rectangular area surrounded by a white dashed line in Fig. 4(a). Inside the rod-like crack, HSFL with average period of 200 nm is observed perpendicular to the irradiated laser polarization. In Fig. 5(b), the grooves of the ripple structure are observed to be deep. To explain the basic interaction mechanism between the incident laser and the SiC surface, we simulate the optical field intensity distribution on the surface during the laser irradiation using 3D FDTD method.

Figure 6 shows the distribution of the simulated optical field intensity on *xy* plane induced by a single crater structure on the surface. SiC is optically transparent at 800 nm (1.55 eV) due to the wide bandgap of 3.2 eV. Figures 6(a) and 6(c) show the simulated results of the system with a 140 nm wide, 700 nm long, and 200 nm deep crater. While Figs. 6(b) and 6(d) show the results of the system with a 100 nm wide, 1500 nm long, and 200 nm deep crater.

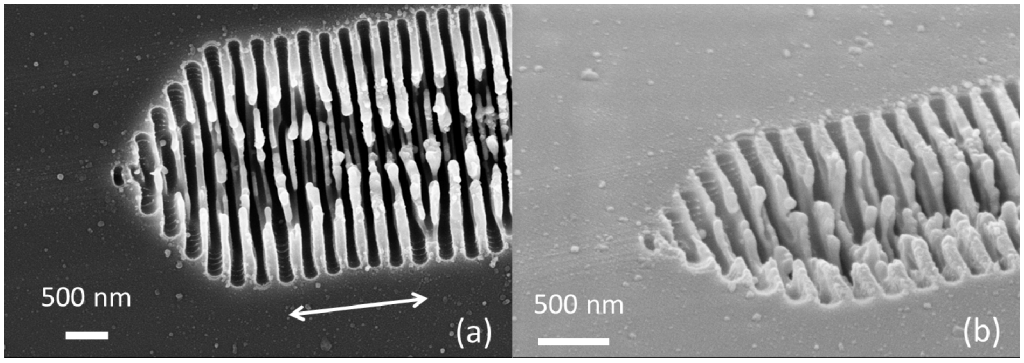

Fig. 5. Magnified SEM images of the area surrounded by the white dashed line in Fig. 4. (a) SEM at normal incidence, (b) SEM at 57 deg. inclined to the surface.

#196394 - $15.00 USD Received 26 Aug 2013; revised 11 Oct 2013; accepted 15 Oct 2013; published 25 Oct 2013

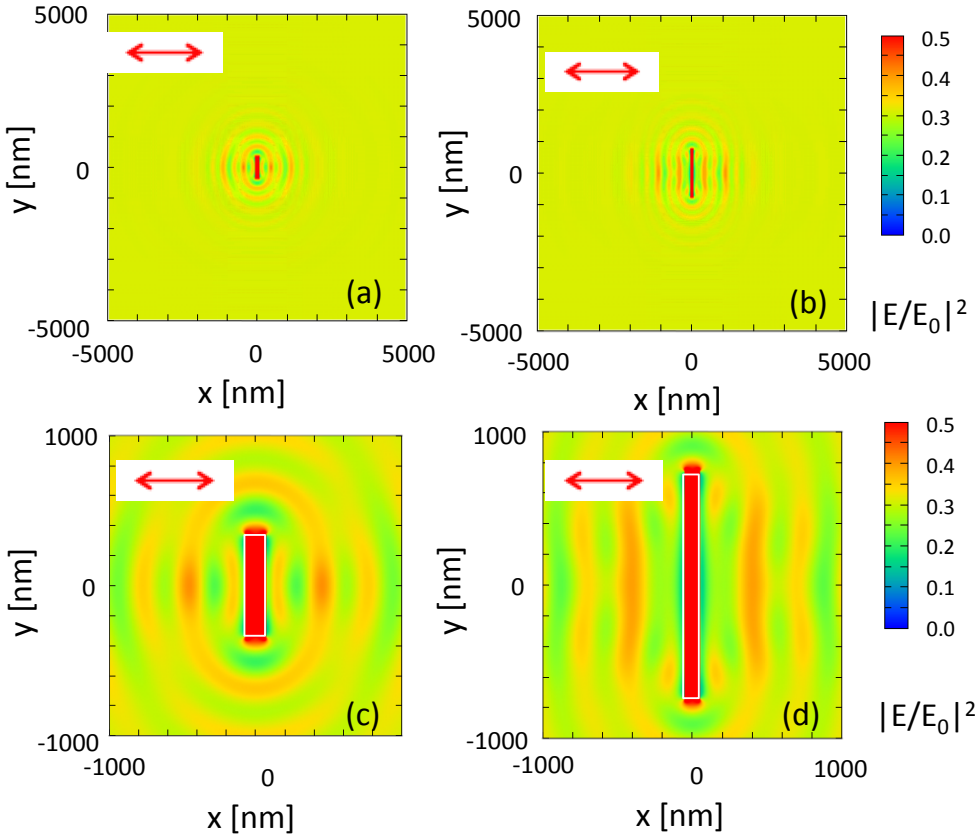

Fig. 6. Distribution of simulated optical field intensity on *xy* plane ($z = -2.5$ nm) induced by a single rod-like crater inside the 4H-SiC. The incident electric field strength is 1 V/m at 800 nm. (a) crater width: 140 nm, length: 700 nm, depth: 200 nm. (b) crater width: 100 nm, length: 1500nm, depth: 200 nm. The magnified images of (a) and (b) are shown in (c) and (d), respectively.

The two systems are to simulate the early stages of HSFL formation. An optical enhancement factor of the entire substrate is lower than unity due to the Fresnel reflection on the substrate surface. Enhanced *near-field* zone with intensity of 0.5 is obtained near the edge of the long direction of the crater structure. This high intensity zone will induce the ablation for HSFL growth perpendicular to the polarization direction. Actually average growth rate of HSFL along the longitudinal crater direction is estimated in experiment to be 48.9 nm/pulse, as will be shown later in Fig. 8. Evaluating the spatial periodicity of the interference pattern from Fig. 6(c), we obtain 240 nm approximately, while the experimental periodicity of the formed HSFL is 200 nm approximately (Fig. 5(a)). The simulated periodicity of the

#196394 - $15.00 USD Received 26 Aug 2013; revised 11 Oct 2013; accepted 15 Oct 2013; published 25 Oct 2013

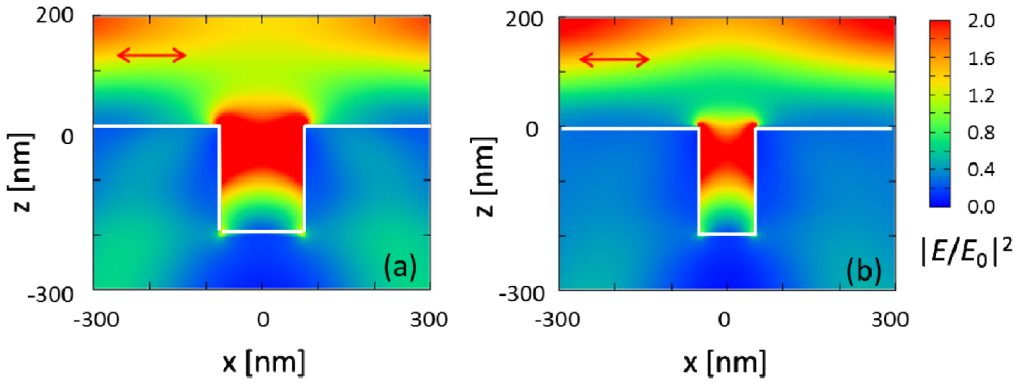

Fig. 7. Distribution of simulated optical field intensity on xz plane induced by single crater inside the 4H-SiC at y = 0 nm. The incident electric field strength is 1 V/m at 800 nm. (a) crater width: 140 nm, length: 700 nm, depth: 200 nm, (b) crater width: 100 nm, length: 1500 nm, depth: 200 nm .White line shows the SiC substrate surface.

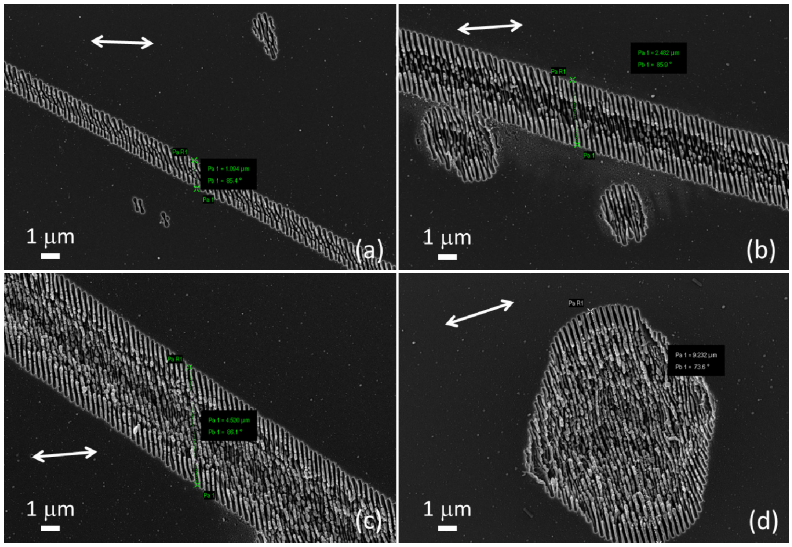

Fig. 8. SEM images of the 4H-SiC surfaces after the femtosecond laser pulse irradiation with constant fluence of 0.3 J/cm^2. (a) 20 pulses, (b) 50 pulses, (c) 100 pulses, and (d) 200 pulses.

interference pattern is close to the experimental result. The deviation would be caused due to multiple-pulse irradiation effects. Electromagnetic wave is propagating perpendicular to the polarization direction. It is the driving energy to increase the number of HSFL perpendicular to the polarization by nanoablation process and HSFL is governed by the scattering far-field distribution. The interference between the incident light and the scattered far-field obtained around the ripples may create the interference pattern of the light intensity distribution.

Figure 7 shows the optical field distribution on xz plane(y = 0). In Figs. 7(a) and 7(b), the highly localized near-field was obtained both in the groove and at outer part. The optical intensity at the bottom of 200 nm deep crater is not large. At the initial stages of 50-nm~100-nm depth a high intensity zone at the bottom surface is obtained. In addition to this enhanced near-field zone, the grating coupling can deepen the groove.

Figure 8 shows SEM images of the 4H-SiC surfaces after the femtosecond laser irradiation with 0.3 J/cm^2. With the increase of the pulse number, an initial crater existing in the center of the beam spot continues to extend in the direction perpendicular to the

#196394 - $15.00 USD Received 26 Aug 2013; revised 11 Oct 2013; accepted 15 Oct 2013; published 25 Oct 2013

polarization. Average growth rate of HSFL along the longitudinal crater direction is estimated to be 48.9 nm/pulse. This average growth rate is estimated by averaging a total growth length of 200 pulse irradiation and averaged 5 experimental measurements. HSFL continues to extend in the direction perpendicular to the polarization. However, it does not grow uniformly in the irradiated spot. This structure has been scattered in the irradiation beam spot. In Fig. 3, structural defects are generated on the substrate surface by the multiple-pulse irradiation of femtosecond laser. We consider the crater and HSFL are formed in a region where the initial defect is induced.

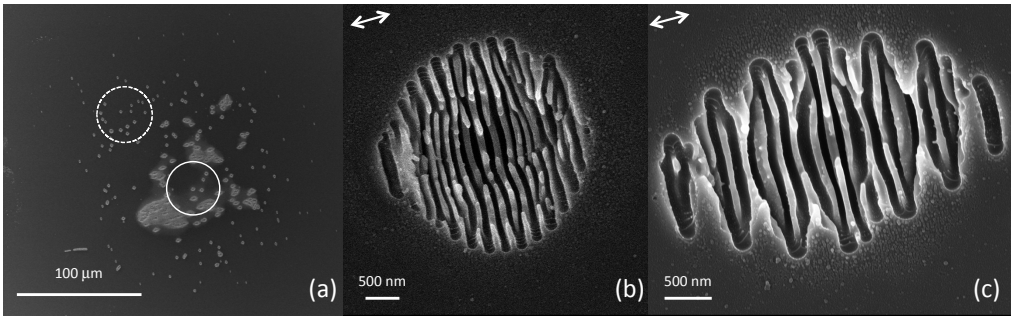

Fig. 9. SEM images of the 4H-SiC surface after the 50 pulse irradiation of femtosecond laser at constant fluence of 0.4 J/cm^2. (a) Total area of the irradiation. (b) Periodic ripples near the edge of the irradiated area, which is in the white *dashed* circle in (a). (c) Periodic ripples in the center of the irradiated area, which is in the white *solid* circle in (a).

Two types of periodic ripples are observed in Fig. 9. Near the edge of the irradiated area, only HSFL structures are formed (Fig. 9(b)), while in the central spot the HSFL is seen *in the LSFL structures* (Fig. 9(c)). SiC has a wide bandgap (3.2 eV) semiconductor while photon energy of 800 nm wavelength is 1.55 eV. Therefore, at an irradiated laser intensity of 2.67 x 10^{12} W/cm^2 (0.4 J/cm^2) two-photon and three-photon excitation processes play a major role in the interaction process. In the central area of the irradiated region high intensity laser easily excites electrons in the valence band into the conduction band. As for the underlying mechanism of LSFL on Si surfaces, Bonse group reported that valence electrons are excited to the conduction band [18]. Silicon exhibits an optical characteristic like metal when the density of free electrons in the conduction band is increased. In this system, Drude model that is an approximated model of the classical Lorentz model of dielectric materials can be used. Dielectric function by the Drude model approximation is written by the following equation:

$$\tilde{\varepsilon}^* = \left(n + ik\right)^2 = \tilde{\varepsilon} + \Delta\tilde{\varepsilon}_{Drude} \tag{1}$$

$$\Delta\tilde{\varepsilon}_{Drude} = \frac{-e^2 N_e}{\varepsilon_0 m^*_{opt} m_e \omega^2 \left[1 + \frac{i}{\omega\tau_D}\right]} \tag{2}$$

where a Drude term is added to the dielectric function. m_e is electron mass, m^*_{opt} is effective mass of 0.4 [37], and τ_D is collision duration of 1.1 fs [18]. Optical constants of SiC were taken from [18,36,37] to calculate dielectric constants for optically excited 4H-SiC substrate. From Eqs. (1) and (2) refractive index n and extinction coefficient k are achieved and shown in Fig. 10.

#196394 - $15.00 USD Received 26 Aug 2013; revised 11 Oct 2013; accepted 15 Oct 2013; published 25 Oct 2013

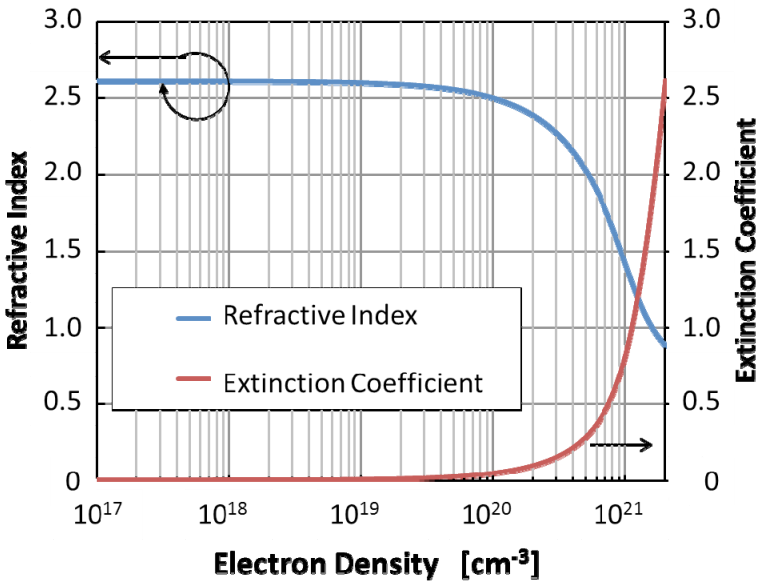

Fig. 10. Refractive index and extinction coefficient as a function of electron density in SiC.

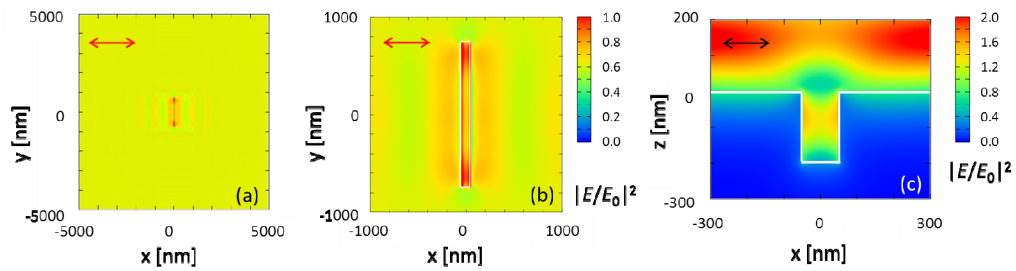

Fig. 11. Optical intensity distribution on exited SiC substrate surface with a crater (width: 100 nm, length: 1500 nm, depth: 200 nm). The incident electric field strength is 1 V/m at 800 nm. (a) *xy* plane, (b) magnified image of (a), and (c) *xz* plane.

The electron density exceeds $N_e = 1\text{x}10^{20}$ cm^{-3}, n and k start to change. At critical density of $N_{cr} = 1.14\text{x}10^{21}\text{cm}^{-3}$ determined by 800 nm wavelength, one gets $n = 1.272$, and $k = 1.028$.

At the critical density, optical intensity distribution on excited SiC substrate with a single crater is simulated by 3D FDTD method, which is shown in Fig. 11. In Figs. 11(a) and 11(b), an optical filed enhancement distribution with periodicity close to the laser wavelength is obtained perpendicular to the incident polarization. These results are consistent with the results reported in [21]. Evaluating the spatial periodicity of the interference pattern from Fig. 11(a), we obtain 930 nm approximately, while the experimental periodicity is 600 nm approximately (Fig. 9(c)). The deviation would be caused due to the large electron density assumed and multiple-pulse irradiation effects. Under the experimental conditions of LSFL fabrication, the electron density in SiC seems to be lower than the critical density ($1.14\text{x}10^{21}\text{cm}^{-3}$) at 800 nm. This periodicity is different from that of non-excited (bare) SiC shown in Fig. 6. This distribution in Fig. 11 is caused by surface plasmonic scattering due to the high density free electrons. It is confirmed that the incident wave and the far field (long-range polaritons) of the surface plasmons are interfered to exhibit interference fringes. The crater acts as a plasmonic scattering source. In Fig. 11(c), high optical enhancement factor is

#196394 - $15.00 USD Received 26 Aug 2013; revised 11 Oct 2013; accepted 15 Oct 2013; published 25 Oct 2013

obtained not at the bottom of the crater but in the crater. The dielectric constant of the SiC substrate is converted into a metal-like nature and surface plasmon scattering becomes dominant in the center rather than Mie scattering in the periphery of the irradiated area, as shown in Fig. 6. Therefore, periodic structures obtained in the center of the crater were LSFL, as evidenced by experimental observation of surface structures (Fig. 9). However, at the edge of the irradiation spot, the electron density is not high enough to exhibit a metal-like nature [21]. Mie scattering is so dominant there that HSFL is predominantly fabricated.

As described above, the periodicity of the ripple is governed by the interference of the incident wavelength and plasmonic scattering wave or Mie scattering wave. In plasmonic case (LSFL) the plasmon wavelength is determined by the metal-like layer and the substrate (under the metal layer), which is generally shorter than the free space wavelength. In Mie scattering regime, the dielectric constant is modulated by the intense fs laser irradiation. Eventually, if one knows the dielectric constant at which the ripple is formed, one can estimate the accurate periodicity of the ripple.

4. Conclusions

The underlying physics of high special frequency periodic ripples (HSFL) fabricated on SiC crystal surfaces by irradiation with femtosecond laser pulses has not been elucidated before. Therefore this paper presented experimentally and theoretically the evolution of HSFL fabricated on SiC crystal surfaces by irradiation with femtosecond laser pulses in a vacuum chamber. We elucidated experimentally and theoretically that Mie scattering from the surface defect is a cause for growing the HSFL. Surface defects were induced after the multiple irradiation of femtosecond laser. HSFL was formed on the periphery. This is attributed to the fact that Mie scattering is dominant when the electron density is low, so that HSFL is predominantly fabricated. These experimental results were well explained by 3D FDTD simulation method.

Acknowledgments

This study was supported by a Grant-in-Aid for Scientific Research (B-23360161) from MEXT Japan. The authors thank Dr. Meng ju Sher and Benjamin Franta of Mazur group for their fruitful discussion. G. Obara is grateful for the JSPS Fellowship for Young Scientists.

#196394 - $15.00 USD Received 26 Aug 2013; revised 11 Oct 2013; accepted 15 Oct 2013; published 25 Oct 2013